

Histogram Monte Carlo Simulation of the Geometrically Frustrated XY Antiferromagnet with Biquadratic Exchange

M.Žukovič^{a*}, T.Idogaki^a and K.Takeda^{a,b}

^a Department of Applied Quantum Physics, Kyushu University

^b Institute of Environmental Systems, Kyushu University

Abstract. Histogram Monte Carlo simulation is used to investigate effects of biquadratic exchange J_2 on phase transitions of a 3D classical XY antiferromagnet with frustration induced by the antiferromagnetic exchange J_1 and the stacked triangular lattice geometry. The biquadratic exchange is considered negative (antiferroquadrupolar) within the triangular planes and positive (ferroquadrupolar) between the planes. The phase diagram obtained features a variety of interesting phenomena arising from the presence of both the biquadratic exchange and frustration. In a strong biquadratic exchange limit ($|J_1|/|J_2| \leq 0.25$), the antiferroquadrupolar phase transition which is of second order is followed by the antiferromagnetic one which can be either first or second order. The separate antiferroquadrupolar and antiferromagnetic second-order transitions are found to belong to the chiral XY and Ising universality classes, respectively. If the biquadratic exchange is reduced both transitions are found to be first order and occur simultaneously in a wide region of $|J_1|/|J_2|$. However, if $|J_2| \rightarrow 0$ the transition changes to the second-order one with the chiral universality class critical behavior.

PACS codes: 75.10.Hk; 75.30.Kz; 75.40.Cx; 75.40.Mg.

Keywords: XY model; Frustrated antiferromagnet; Biquadratic exchange; Phase transition; Quadrupole ordering; Histogram Monte Carlo simulation;

*Corresponding author.

Permanent address: Institute of Environmental Systems, Faculty of Engineering, Kyushu

University, Fukuoka 812-8581, Japan

Tel.: +81-92-642-3811; Fax: +81-92-633-6958

E-mail: milantap@mbox.nc.kyushu-u.ac.jp

I. Introduction

The problem of biquadratic or generally higher-order exchange interactions in systems with Heisenberg symmetry has been addressed in several mean field approximation (MFA) studies¹⁻³, by high-temperature series expansion (HTSE) calculations⁴, as well as within a framework of some other approximative schemes^{5,6}. It has been shown that such interactions can induce various interesting properties such as tricritical and triple points, quadrupole ordering, separate dipole and quadrupole phase transitions etc. Much less attention, however, has been paid to this problem on systems with XY spin symmetry. Chen *et.al*^{7,8} calculated transition temperatures and the susceptibility critical indices for an XY ferromagnet with biquadratic exchange on cubic lattices by the HTSE method for limited region of J_1/J_2 . However, the rigorous proof of the existence of dipole long-range order (DLRO), corresponding to the ferromagnetic directional arrangement of spins, and quadrupole long-range order (QLRO), representing an axially ordered state in which spins can point in either direction along the axis of ordering, at finite temperature on the classical bilinear-biquadratic exchange model has only recently been provided independently by Tanaka and Idogaki⁹, and Campbell and Chayes¹⁰. Very recently we have considered the XY model with the bilinear-biquadratic exchange Hamiltonian on a simple cubic¹¹ and hexagonal (stacked triangular)¹² lattices, and performed a finite-size scaling (FSS) analysis in order to investigate critical properties of the considered systems via Standard Monte Carlo (SMC) and Histogram Monte Carlo (HMC) simulations.

So far, however, to our best knowledge there has been no investigation of the effect of the biquadratic exchange on an XY model with frustrated/competing exchange interaction. In this paper we present systematic investigations of the role of the biquadratic exchange in phase transitions of the geometrically frustrated XY antiferromagnet on stacked triangular lattice (STL). This model has been argued to possess some unique properties such as novel chiral universality class critical behavior^{13,14}, but many more remarkable features have been observed when the effects of external magnetic field¹⁵ and next-nearest neighbors¹⁶ were considered. In the present work, the effect of the biquadratic exchange is also found to bring about variety of interesting phenomena, such as regions of first order transitions, separate magnetic and quadrupolar ordering, transitions of different universality classes, etc.

II. Model and computation details

We consider the XY model, described by the Hamiltonian

$$H = -J_1 \sum_{\langle i,j \rangle} \mathbf{S}_i \cdot \mathbf{S}_j - J_2^\perp \sum_{\langle i,k \rangle} (\mathbf{S}_i \cdot \mathbf{S}_k)^2 - J_2^\parallel \sum_{\langle i,l \rangle} (\mathbf{S}_i \cdot \mathbf{S}_l)^2, \quad (1)$$

where $\mathbf{S}_i = (S_i^x, S_i^y)$ is a two-dimensional unit vector at the i th lattice site and the sums $\langle i, j \rangle$, $\langle i, k \rangle$ and $\langle i, l \rangle$ run over all nearest neighbors (NN), NN in the xy -plane, and NN in the stacking z -axis direction, respectively. We consider the bilinear exchange interaction $J_1 < 0$, the biquadratic intra-plane and inter-plane exchange interactions $J_2^\perp < 0$ and $J_2^\parallel > 0$, respectively, with $|J_2^\perp| = |J_2^\parallel| = |J_2|$.

Assuming periodic boundary condition, spin systems of the linear lattice sizes $L = 12, 18, 24$ and 30 are first used in SMC simulations. For a fixed value of the exchange ratio $|J_1|/|J_2|$, we start the simulation process at low (high) temperatures from an antiferromagnetic/random (random) initial configuration and gradually raise (lower) temperature. These heating-cooling loops serve to check possible hysteresis, accompanying first-order transitions. As we move in $(|J_1|/|J_2|, k_B T/|J_2|)$ space, we use the last spin configuration as an input for calculation at the next point. We sweep through the spins in sequence and updating follows a Metropolis dynamics. In the updating process, the new direction of spin in the spin flip is selected completely at random, without any limitations by a maximum angle of spin rotation or allowed discrete set of resulting angle values. Thermal averages at this stage are calculated using at most 1×10^5 Monte Carlo steps per spin (MCS/s) after thermalizing over another 0.5×10^5 MCS/s. We calculate the system internal energy E and some other physical quantities defined as follows: the specific heat per site c

$$c = \frac{(\langle E^2 \rangle - \langle E \rangle^2)}{N k_B T^2}, \quad (2)$$

the dipole LRO (DLRO) parameter m ,

$$m = \frac{\langle M \rangle}{N} = \frac{1}{N} \left\langle \sqrt{6 \sum_{\alpha=1}^6 \mathbf{M}_\alpha^2} \right\rangle, \quad (3)$$

where \mathbf{M}_α is the α th sublattice-magnetization vector (note that the present model has six equivalent magnetic sublattices), given by

$$\mathbf{M}_\alpha = \left(\sum_i S_{\alpha i}^x, \sum_i S_{\alpha i}^y \right), \quad (4)$$

the quadrupole LRO (QLRO) parameter q ,

$$q = \frac{\langle Q \rangle}{N} = \frac{1}{N} \left\langle \sqrt{6 \sum_{\alpha=1}^6 Q_{\alpha}^2} \right\rangle , \quad (5)$$

where

$$\mathbf{Q}_{\alpha} = \left(\sum_i \left((S_{\alpha i}^x)^2 - (S_{\alpha i}^y)^2 \right), \sum_i 2S_{\alpha i}^x S_{\alpha i}^y \right) , \quad (6)$$

the chiral LRO (CHLRO) parameter κ ,

$$\kappa = \frac{\sqrt{\langle K^2 \rangle}}{N} = \frac{1}{N} \sqrt{\left\langle \left(\sum_p \kappa_p \right)^2 \right\rangle} , \quad (7)$$

where the summation runs over all upward triangles on the triangular layer and κ_p represents a local chirality at each elementary triangular plaquette, defined by

$$\kappa_p = \frac{2}{3\sqrt{3}} \sum_{\langle i,j \rangle}^p [\mathbf{S}_i \times \mathbf{S}_j]_z = \frac{2}{3\sqrt{3}} [\sin(\varphi_2 - \varphi_1) + \sin(\varphi_3 - \varphi_2) + \sin(\varphi_1 - \varphi_3)] , \quad (8)$$

where the summation runs over the three directed bonds surrounding each plaquette, p , and φ_i represents the i th spin angle. κ_p is an Ising-like quantity representing the sign of rotation of the spins along the three sides of each plaquette. Further, the following quantities which are functions of the parameter O ($= M, Q, K$) are defined: the susceptibility per site χ_O

$$\chi_O = \frac{(\langle O^2 \rangle - \langle O \rangle^2)}{Nk_B T} , \quad (9)$$

the logarithmic derivatives of $\langle O \rangle$ and $\langle O^2 \rangle$ with respect to $\beta = 1/k_B T$

$$D_{1O} = \frac{\partial}{\partial \beta} \ln \langle O \rangle = \frac{\langle OE \rangle}{\langle O \rangle} - \langle E \rangle , \quad (10)$$

$$D_{2O} = \frac{\partial}{\partial \beta} \ln \langle O^2 \rangle = \frac{\langle O^2 E \rangle}{\langle O^2 \rangle} - \langle E \rangle , \quad (11)$$

the fourth-order long-range order cumulant U (Binder parameter)

$$U = 1 - \frac{\langle O^4 \rangle}{3\langle O^2 \rangle^2} , \quad (12)$$

and the fourth-order energy cumulant V

$$V = 1 - \frac{\langle E^4 \rangle}{3\langle E^2 \rangle^2} . \quad (13)$$

The above quantities are useful for localization of a transition as well as for determination of its nature. For example, first-order transitions usually manifest themselves by discontinuities in the order parameter and energy, and hysteresis when cooling and heating. If transition is second order, it can be localized approximately by the χ_O peak position or more precisely by the intersection of the fourth-order LRO (or energy) cumulants curves for different L .

In order to increase precision and reliability of the obtained information, as well as to retrieve some additional information which could not be extracted from the SMC calculations, we further perform HMC calculations, developed by Ferrenberg and Swendsen^{17,18}, at the estimated transition temperatures for each lattice size. Here, 2×10^6 MCS/s are used for calculating averages after discarding another 1×10^6 MCS/s for thermalization. We calculate the energy histogram $P(E)$, the order parameters histograms $P(O)$ ($O = M, Q, K$), as well as the physical quantities (2)-(13). Using data from the histograms, one can calculate physical quantities at neighboring temperatures, and thus determine the values of extrema of various quantities and their locations with high precision for each lattice size. In such a way we can obtain quality data for FSS analysis which determines the order of the transition and, in the case of a second-order transition, it also allows us to extract critical indices. For example, the energy cumulant V exhibits a minimum near critical temperature T_c , which achieves the value $V^* = \frac{2}{3}$ in the limit $L \rightarrow \infty$ for a second-order transition, while $V^* < \frac{2}{3}$ is expected for a first-order transition^{17,18}. Temperature-dependences of a variety of thermodynamic quantities display extrema at the L -dependent transition temperatures, which at a second-order transition are known to scale with a lattice size as, for example:

$$\chi_{O,max}(L) \propto L^{\gamma_O/\nu_O} , \quad (14)$$

$$D_{1O,max}(L) \propto L^{1/\nu_O} , \quad (15)$$

$$D_{2O,max}(L) \propto L^{1/\nu_O} , \quad (16)$$

where ν_O and γ_O represent the correlation length and susceptibility critical indices, respectively. In the case of a first-order transition (except for the order parameters), they display a volume-dependent scaling, $\propto L^3$. The simulations were performed on the vector supercomputer FUJITSU VPP700/56.

III. Chirality on frustrated quadrupoles

It has been known for some time that the frustrated spin system on triangular lattice possesses the chirality κ as defined in Eqns.(7,8)¹⁹. Due to the chirality the system has two-fold degeneracy of the ground state ($\kappa = +1$ and $\kappa = -1$), resulting in the structure with spins arranged on plaquettes with turn angles $+120^\circ$ and -120° , respectively (Fig.1(a)). A minimum energy condition is realized by an arrangement in which the $+$ and $-$ plaquettes alternate, producing long-range chiral order at low temperatures. Such a system has been argued to belong to a nonstandard universality class linked to the two-fold chiral degeneracy inherent to the 120° ordered spin structure^{13,14}, the critical behavior of which is characterized by critical indices, different from those for non-frustrated systems with the same spin symmetry. Since the present Hamiltonian includes both bilinear and biquadratic terms, let us take a closer look at the opposite side of the exchange ratio spectrum and investigate critical behavior of the system with only biquadratic exchange interaction, i.e. the case of $J_1 = 0$. If $J_2^\perp < 0$ (the sign of J_2^\parallel is irrelevant in the present consideration) the quadrupolar system is frustrated due to the triangular lattice geometry, resulting in a non-collinear ground state. The non-collinear ground state arrangement resembles the 120° structure of the antiferromagnetic system, however, here, the spins can point in either direction within the given axis (for illustration see the snapshots in Fig.12). As far as the chirality κ is concerned, such a system has four-fold degeneracy in the ground state of each plaquette ($\kappa_p = \pm 1, \pm \frac{1}{3}$), resulting in the structure with four possible turn angles between two neighboring spins $\pm 120^\circ, \pm 60^\circ$. However, there is no energetically favorable arrangement among the four kinds of plaquettes and, hence, the plaquettes do not order even at low temperatures. Nevertheless, even for such a system we can define the quantity analogous to the chirality of the antiferromagnetic system (let us call it the quadrupolar chirality) if we consider instead of spins their axes and turn angles between the axes, which are again $\pm 120^\circ$. If we define the local quadrupolar chirality as

$$\kappa_p^q = \frac{2}{3\sqrt{3}}[\sin 2(\varphi_2 - \varphi_1) + \sin 2(\varphi_3 - \varphi_2) + \sin 2(\varphi_1 - \varphi_3)] , \quad (17)$$

and the quadrupolar chirality LRO parameter (QCHLRO) κ^q as

$$\kappa^q = \frac{\sqrt{\langle (K^q)^2 \rangle}}{N} = \frac{1}{N} \sqrt{\left\langle \left(\sum_p \kappa_p^q \right)^2 \right\rangle} , \quad (18)$$

concerning such defined quadrupolar chirality, the system will have two-fold degeneracy of the ground state ($\kappa^q = -1$ and $\kappa^q = +1$, corresponding to turn angles $+120^\circ$ and -120° ,

respectively (Fig.1(b))), and the situation will much resemble the one for the antiferromagnetic system with the chirality κ . Furthermore, in analogy with the chirality κ which is believed to order along with spins, here, the quadrupolar chirality κ^q is expected to show LRO simultaneously with quadrupoles.

IV. FSS analysis and phase diagram

We first consider the case of $J_2 = 0$. To determine the order of the transition we analyze the scaling behavior of the minimal value of the energy cumulant V at the transition temperature. As shown in Fig.2, V tends to the value of $2/3$, as expected for a second-order transition, and the slope 2.39 means that V is not volume dependent. Also, observing the energy and LRO parameters distribution histograms (not shown), no bimodal distribution, which would signal a first-order transition, is found. Hence, both spin and chirality ordering transitions seem to be clearly of second order. The transition temperature, calculated from the intersection of the Binder parameter curves for different L , is estimated to $k_B T_c / |J_1| = 1.4580 \pm 0.0005$, in agreement with the values quoted in Refs.^{13,16}. The chirality transition temperature $k_B T_c^\kappa / |J_1| = 1.4590 \pm 0.0013$, similarly as in Ref.¹³, seems to be slightly higher than the spin ordering temperature but the two values cannot be distinguished beyond the error bar and, hence, we assume they are the same. The spin and chirality critical indices calculated from the scaling relations (14)-(16) take the following values: $\nu_M = 0.52 \pm 0.03$, $\gamma_M = 1.08 \pm 0.08$ and $\nu_K = 0.55 \pm 0.01$, $\gamma_K = 0.81 \pm 0.03$ ²⁵, respectively (Figs.3,4). Also the values of the critical indices are in fair agreement with the two previous studies^{13,16}, however, as far as the universality class is concerned the situation here is not so straightforward and will be discussed later.

The order of the transitions changes, however, when even a comparatively weak bi-quadratic exchange interaction is introduced. Although it is very hard to observe the typical first-order behavior for small values of $|J_2|$, if the lattice sizes are taken sufficiently large the signs of the discontinuous transition show up. This is seen in Fig.5 in which the bimodal (double-peak) energy distribution becomes clearly recognizable if $L \geq 30$, for the case of $|J_2|/|J_1| = \frac{1}{5}$. As $|J_2|$ is increased, the first-order features of the transition are becoming more and more apparent. Fig.6 shows clearly bimodal energy distribution histograms for $|J_1|/|J_2| = 1.3$, in which the dip between the peaks is observable already at smaller L , quite

rapidly approaching zero as L is increased, indicating discontinuous behaviour of the energy at a rather strong first-order transition. Although we do not show it here, similar double peaks can also be observed in the histograms of each LRO parameter.

The transition remains first order and simultaneous for dipole, quadrupole and chiralities ordering until fairly small values of $|J_1|/|J_2|$. Below $|J_1|/|J_2| \simeq 0.25$, however, quadrupoles order separately at temperatures higher than those for dipole ordering. Thus the phase boundary branches and a new middle phase of axial quadrupole long-range order (QLRO) without magnetic dipole ordering opens between the paramagnetic and DLRO phases. This phase broadens as $|J_1|/|J_2|$ decreases, since the QLRO branch is little sensitive to the $|J_1|/|J_2|$ ratio variation and levels off, while the DLRO branch turns down approaching the point $(|J_1|/|J_2|, k_B T/J_2) = (0, 0)$. This means that the ground state is always magnetic as long as there is a finite dipole exchange interaction. In Fig.7 we present the temperature variation of the DLRO, QLRO, CHLRO and QCHLRO parameters m , q , κ and κ^q , respectively, at $|J_1|/|J_2| = 0.15$. We can see that quadrupoles order before dipoles, forming a fairly broad region of QLRO without DLRO. On the other hand, the chirality and quadrupole chirality seem to order simultaneously with dipoles and quadrupoles, respectively. The QLRO transition is apparently second order down to $|J_1|/|J_2| = 0$ and the critical indices take the values $\nu_Q = 0.50 \pm 0.03$, $\gamma_Q = 1.09 \pm 0.08$ at $|J_1|/|J_2| = 0.15$ (Fig.8) and $\nu_Q = 0.520 \pm 0.003$ and $\gamma_Q = 1.072 \pm 0.009$ at $J_1 = 0$. In the case of $J_1 = 0$, the QLRO transition temperature is located as $k_B T_q/J_2 = 0.729 \pm 0.002$. On the other hand, in the case of the DLRO transition, the first order seems to persist even after the QLRO and DLRO boundaries separate for a small range of the exchange ratio values just below the splitting point. This is clearly seen in Fig.9 from the distribution diagrams of the DLRO and QLRO parameters. Although at first glance it seems that both transitions occur at the same temperature and are of first order, a closer look reveals that while the bimodal distribution of the DLRO parameter is between the disordered and ordered states, the bimodal distribution of the QLRO parameter is between two ordered states of different finite QLRO parameter values. Therefore, here, the QLRO parameter only shows a discontinuity within the QLRO region, rather than paramagnetic-QLRO transition. The first-order DLRO transition changes to the second-order one upon further lowering of $|J_1|/|J_2|$. This is seen from the finite-size scaling analysis of the HMC data for $|J_1|/|J_2| = 0.15$ (Fig.10). The slopes apparently indicate the second-order character

of the transition with the critical indices $\nu_M = 0.63 \pm 0.02$, $\gamma_M = 1.25 \pm 0.04$. The resulting phase diagram is drawn in Fig.11 and some relevant numerical results listed in Table 1.

V. Summary and discussion

We studied effects of the biquadratic exchange on the phase diagram of the frustrated classical XY antiferromagnet on STL. This study, which to our best knowledge is first for the studied system, covered most of the significant phenomena induced by the presence of the biquadratic exchange, and present a fairly compact picture of the role of this higher-order exchange interaction on the critical behaviour of the system considered. We obtained the phase diagram with two ordered phases: in the region where the bilinear exchange is dominant there is a single phase transition to the DLRO phase, which is second order at $J_2 = 0$, but changes to a first-order one upon adding of a rather small amount of biquadratic exchange. In the region of small $|J_1|/|J_2|$ the phase boundary splits into the QLRO transition line at higher temperatures and the DLRO transition line at lower temperatures, which are second order, and partly first and partly second order, respectively.

From our qualitative and quantitative evaluations we found out that not only the order of the transitions in different regions of the $|J_1|/|J_2|$ parameter is not the same, but also the sets of the critical indices obtained in different regions of the second-order transition are different for seemingly the same kind of transition while almost identical for different kinds of transition. Let us first discuss the problem of the order of the transition. The second-order transition at $J_2 = 0$ is in agreement with the previous MC studies^{13,16} but in contradiction with the renormalization group study²⁰, which predicts a clear first-order transition. At finite J_2 , the first-order transition observed in the region of the paramagnetic-DLRO transition has also been observed in the case of a ferromagnet with $J_1 > 0$, $J_2^\perp > 0$ and $J_2^\parallel > 0$, however, only in a quite narrow region of $J_1/J_2 \in (0.33, 0.55)$ ¹². We believe that the mechanism responsible for this transition in the present case is similar to that in the case of the ferromagnet, i.e., it could result from a kind of tension between the bilinear and biquadratic exchange interactions, which in the present case seems to be enhanced by the presence of the frustration and consequently causing broadening of the first-order transition region. Namely, while the decreasing bilinear exchange drives the transition temperature down to the lower values, the biquadratic exchange does not follow this tendency

and rather prevents the ordering temperature from rapid decrease. This tendency is clearly seen from the phase diagram both in the region of separate transitions, where T_q does not vary much with decreasing $|J_1|/|J_2|$, as well as in the region of simultaneous ordering, where the transition temperature is apparently enhanced by the presence of the biquadratic exchange (the case of absent biquadratic exchange is represented by the dash-dot straight line in $(|J_1| - k_B T_c)$ parameter space). Put differently, quadrupoles would prefer ordering at higher temperatures but as long as there is a single transition they are prevented to do so by too low bilinear exchange, and order occurs only if the temperature is lowered still further. This “frustration” results in a first-order transition when the strength of the quadrupole ordering prevails and frustrated quadrupoles order abruptly along with dipoles. However, when $|J_2|$ reaches high values the frustration becomes too high for the two kinds of ordering to occur simultaneously and they separate. In order to understand the first-order DLRO transition and QLRO parameter discontinuity in the region just below the point of the separation, we analyzed snapshots (not shown) for $|J_1|/|J_2| = 0.25$ just before the DLRO sets in. In the snapshots we could observe fairly large clusters of antiferromagnetically ordered spins along the stacking direction, which is non-frustrated and in which spins seem to order more easily than within frustrated planes (Note that in the case of the non-frustrated parallel (ferromagnetic) ordering the transition temperature is roughly twice as higher as in the present case¹²). These clusters reorient at the transition as a whole, and such a way may produce discontinuities in the order parameter and internal energy i.e., a first-order transition. Besides those clusters, we could also observe smaller intra-plane clusters of spins the axes of which show local parallel ordering. At the DLRO transition, the spins in these clusters (and also their axes) reorient into the 120° spin structure, which may result in the small discontinuity of the QLRO parameter, seen in Fig.9. The separate QLRO is apparently second order, in agreement with the mapping arguments of Carmesin²¹.

Now, let us address the problem of the critical indices in the case of a second-order transition. For the case of $J_2 = 0$, there has been an argument about the universality class of the critical behavior of such a system. Kawamura claimed that it should display a nonstandard (chiral) universality class behavior due to a two-fold discrete degeneracy Z_2 associated with the two chiral states, with the novel indices ($\alpha_M = 0.34 \pm 0.06$, $\beta_M = 0.253 \pm 0.01$, $\gamma_M = 1.13 \pm 0.05$ and $\nu_M = 0.54 \pm 0.02$)¹³, while Plumer *et al.*²² maintained that there is no

new universality class and that the indices take the mean-field tricritical values ($\alpha_M = \frac{1}{2}$, $\beta_M = \frac{1}{4}$, $\gamma_M = 1$ and $\nu_M = \frac{1}{2}$). As we can see, the DLRO critical indices obtained from our calculations $\nu_M = 0.52 \pm 0.03$, $\gamma_M = 1.08 \pm 0.08$ are somewhere between those from Refs.^{13,22} and, considering the error estimates, could be interpreted for support of either of the theories. Although we can make no definite conclusion based on the values of the indices themselves, we believe that the former interpretation is more favorable. Indeed, looking at the critical indices of the separate QLRO transitions we can see that they are strikingly similar to those for the case of $J_2 = 0$ (and seem to be such along the whole paramagnetic-QLRO boundary). These indices can hardly be interpreted as the mean-field tricritical ones and the theory of the same universality class critical behavior of quadrupoles ($J_1 = 0$) and dipoles ($J_2 = 0$), based on mapping and quantitative analysis²³, would rather strongly suggest that both cases show the chiral universality class behavior. As far as the separate DLRO transition is concerned, in the second-order transition region we obtained the critical indices $\nu_M = 0.63 \pm 0.02$, $\gamma_M = 1.25 \pm 0.04$, which are quite different from those for the DLRO transition at $J_2 = 0$. The reason is that in this case the transition has an Ising-like character and, hence, the indices take on the Ising universality class values ($\nu^{Ising} = 0.629$, $\gamma^{Ising} = 1.239$ ²⁴). The situation is illustrated in Figs.12(a,b). In the QLRO (and no DLRO) region, there is an axial quadrupole ordering on each of the three sublattices (Fig.12(a)) and only upon further lowering of the temperature the system reaches the QLRO+DLRO phase in which the Ising-like directional dipole ordering within the given axis in each sublattice takes place (Fig.12(b)). Therefore, here, the only difference from the Ising case is that dipoles can order along any of the three axes, not only the z-axis.

Our further intention is to perform similar simulations on the STL antiferromagnet for some other interesting cases, like: $J_2^\perp < 0$, $J_2^\parallel < 0$; $J_2^\perp > 0$, $J_2^\parallel > 0$; $J_2^\perp > 0$, $J_2^\parallel < 0$. Besides the geometrical frustration, such spin systems will possess additional frustration arising from the bilinear and biquadratic exchanges competing in the stacking direction, intra-plane direction, and both stacking and intra-plane directions, respectively.

-
- ¹ J. Sivardiere, *Phys. Rev. B* **6**, 4284, (1972).
- ² J. Sivardiere, A.N. Berker and M. Wortis, *Phys. Rev. B* **7**, 343, (1973).
- ³ H.H. Chen and P. Levy, *Phys. Rev. Lett.* **27**, 1383, (1971); *Phys. Rev. B* **7**, 4267, (1973).
- ⁴ H.H. Chen and P. Levy, *Phys. Rev. B* **7**, 4284, (1973).
- ⁵ R. Micnas, *J. Phys. C: Solid St. Phys.* **9**, 3307, (1976).
- ⁶ G.S. Chaddha and A. Sharma, *J. Magn. Magn. Mater.* **191**, 373, (1999).
- ⁷ K.G. Chen, H.H. Chen, C.S. Hsue and F.Y. Wu, *Physica* **87A**, 629, (1977).
- ⁸ K.G. Chen, H.H. Chen and C.S. Hsue, *Physica* **93A**, 526, (1978).
- ⁹ A. Tanaka and T. Idogaki, *J. Phys. Soc. Japan* **67**, 604, (1998).
- ¹⁰ M. Campbell and L. Chayes, *J. Phys. A* **32**, 8881, (1999).
- ¹¹ H. Nagata, M.Žukovič and T. Idogaki, *J. Magn. Magn. Mater.* **234**, 320, (2001).
- ¹² M.Žukovič, T. Idogaki and K. Takeda, *Physica B* **304**, 18, (2001).
- ¹³ H. Kawamura, *J. Phys. Soc. Japan* **54**, 3220, (1985); **55**, 2095, (1986); **56**, 474, (1986); **58**, 584, (1989); **61**, 1299, (1992).
- ¹⁴ H. Kawamura, *Phys. Rev.* **B38**, 4916, (1988); **B42**, 2610 (E), (1990); *J. Phys. Soc. Japan* **59**, 2305, (1990).
- ¹⁵ M.L. Plumer, A. Mailhot and A. Caillé, *Phys. Rev. B* **48**, 3840, (1993).
- ¹⁶ E.H. Boubcheur, D. Loison and H.T. Diep, *Phys. Rev. B* **54**, 4165, (1996).
- ¹⁷ A.M. Ferrenberg and R.H. Swendsen, *Phys. Rev. Lett.* **61**, 2635, (1988).
- ¹⁸ A.M. Ferrenberg and R.H. Swendsen, *Phys. Rev. Lett.* **63**, 1195, (1989).
- ¹⁹ S. Miyashita and H. Shiba, *J. Phys. Soc. Japan* **53**, 1145, (1984).
- ²⁰ A. Antonenko and A. I. Sokolov, *Phys. Rev. B* **49**, 15901, (1994).
- ²¹ H.-O. Carmesin, *Phys. Lett. A* **125**, 294, (1987).
- ²² M.L. Plumer and A. Mailhot, *Phys. Rev. B* **50**, 16113, (1994).
- ²³ M.Žukovič, T. Idogaki and K. Takeda, *Phys. Rev. B* **63**, 172412-1, (2001).
- ²⁴ A.M. Ferrenberg and D.P. Landau, *Phys. Rev. B* **44**, 5081, (1991).
- ²⁵ The errors for ν_O and γ_O are calculated from standard errors of the respective slopes b in the linear regression $y = a + bx$.

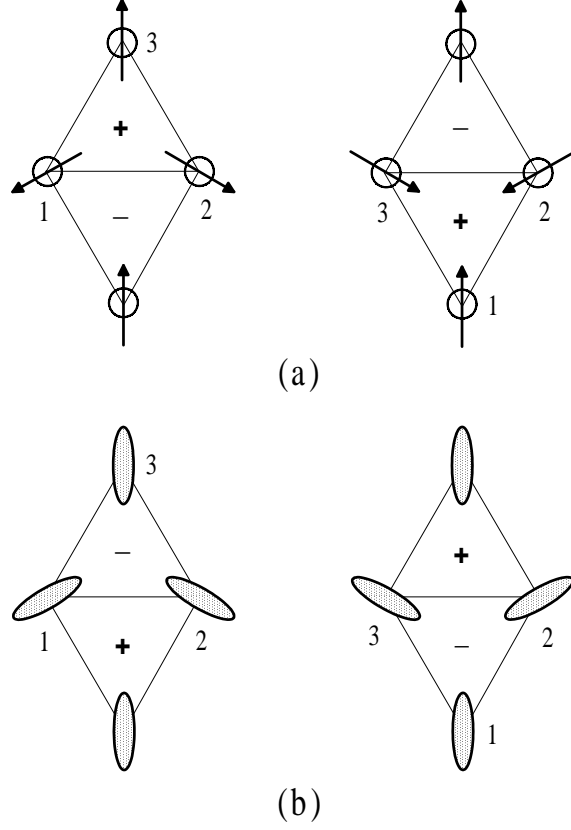


FIG. 1: Two degenerate ground states, $+120^\circ$ and -120° structures on (a) spin and (b) quadrupole plaquettes. Signs $+$ and $-$ denote the sign of (a) chirality and (b) quadrupole chirality of the elementary triangles. Spins and quadrupoles are numbered counterclockwise, corresponding to the definitions (8) and (17).

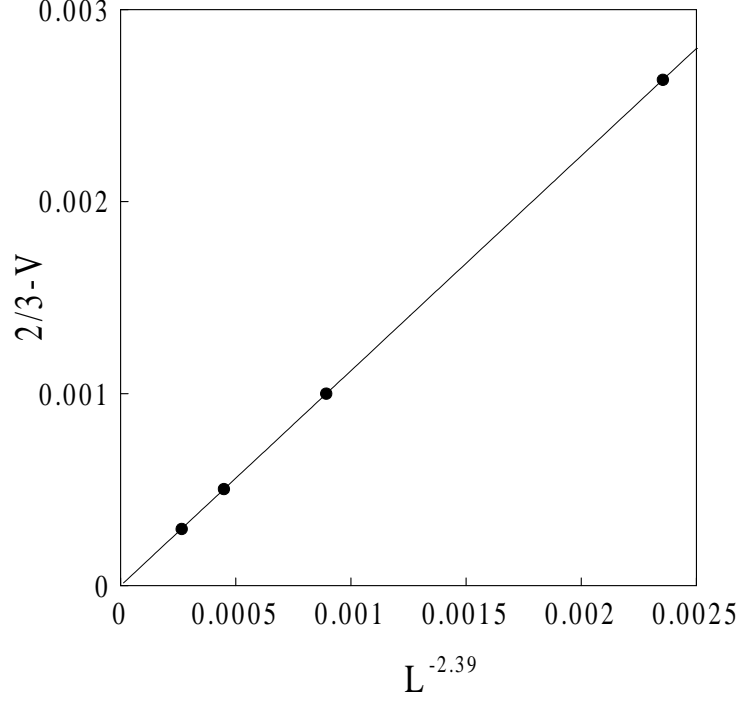


FIG. 2: Scaling of the energy cumulant minima at $J_2 = 0$. The values extrapolated to $L \rightarrow \infty$ approach the value $V^* = \frac{2}{3}$ and do not scale with volume, as it should be in the case of a second-order transition.

TABLE I: Critical indices and transition temperatures for quadrupole, dipole, and chiral ordering, respectively.

$ J_1 / J_2 $	ν_Q	γ_Q	$k_B T_q$
0	0.520 ± 0.003	1.072 ± 0.009	$0.729 \pm 0.002 J_2 $
0.15	0.50 ± 0.03	1.09 ± 0.08	$0.731 \pm 0.001 J_2 $
	ν_M	γ_M	$k_B T_c$
0.15	0.63 ± 0.02	1.25 ± 0.04	$0.523 \pm 0.002 J_2 $
∞	0.52 ± 0.03	1.08 ± 0.08	$1.4580 \pm 0.0005 J_1 $
	ν_κ	γ_κ	$k_B T_\kappa$
∞	0.55 ± 0.01	0.81 ± 0.03	$1.4590 \pm 0.0013 J_1 $

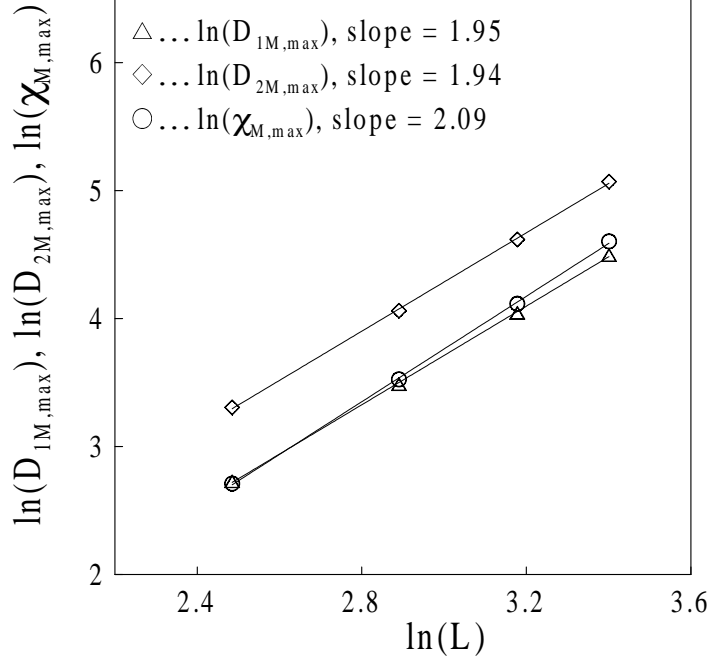


FIG. 3: Scaling behaviour of the maxima of the susceptibility $\chi_{M,max}$ corresponding to the parameter M and logarithmic derivatives of its first and second moments $D_{1M,max}$ and $D_{2M,max}$, respectively, in \ln - \ln plot, for $J_2 = 0$. The slopes yield values of $1/\nu_M$ for $D_{1M,max}$, $D_{2M,max}$ and γ_M/ν_M for $\chi_{M,max}$.

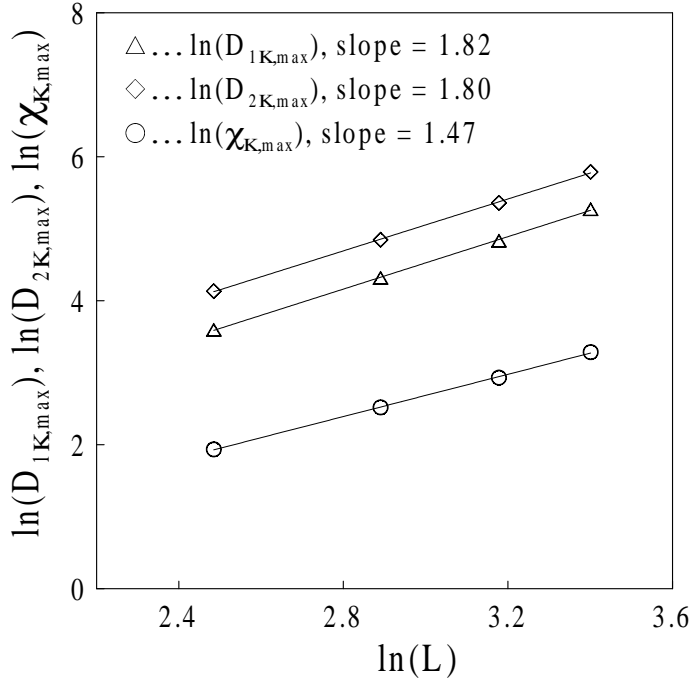


FIG. 4: The same dependence as in Fig.3, with the parameter K considered instead of M .

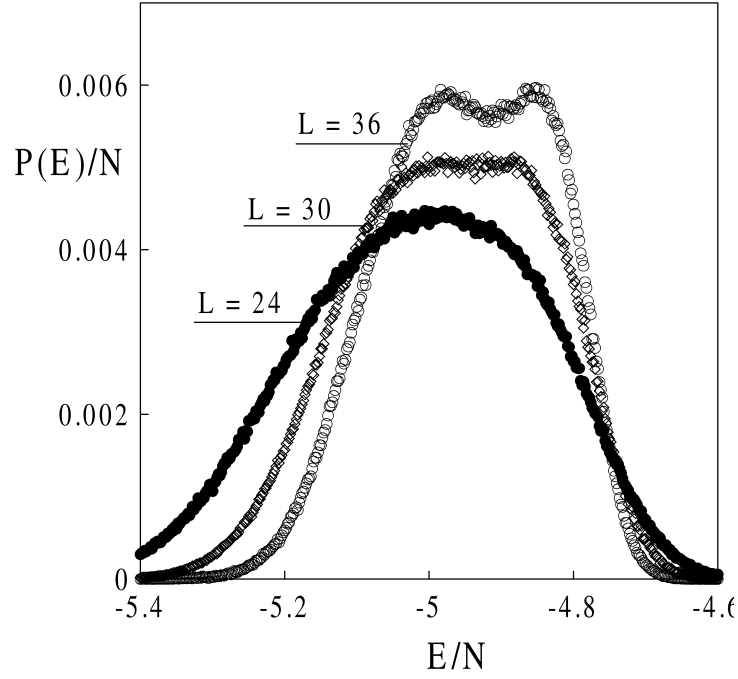


FIG. 5: Energy distribution at the size-dependent transition temperatures $T_c(L)$ for various lattice sizes and $|J_2|/|J_1| = \frac{1}{5}$. The bimodal distribution signaling a first-order transition can only be seen at $L \geq 30$.

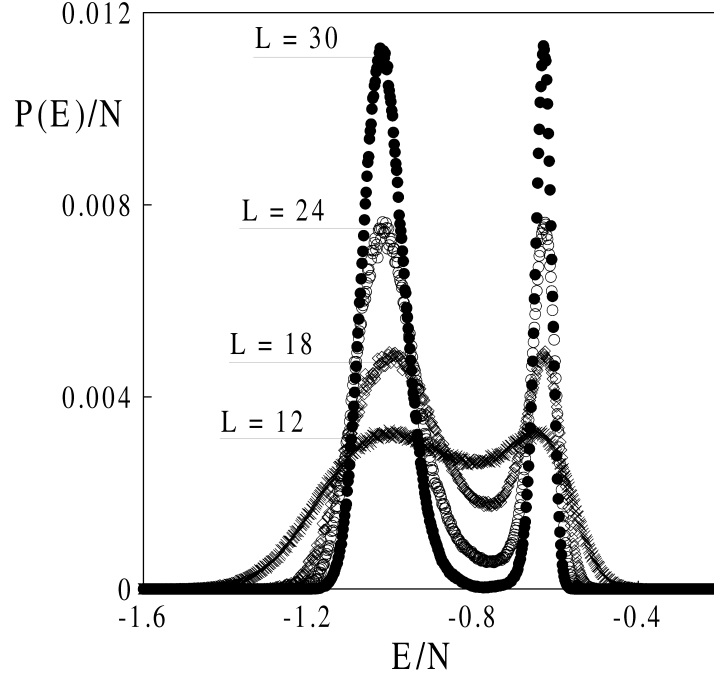


FIG. 6: Energy distribution at $T_c(L)$ for $|J_1|/|J_2| = 1.3$. Double-peaked structure with deepening barrier between the two energy states with increasing lattice size indicates a first-order transition.

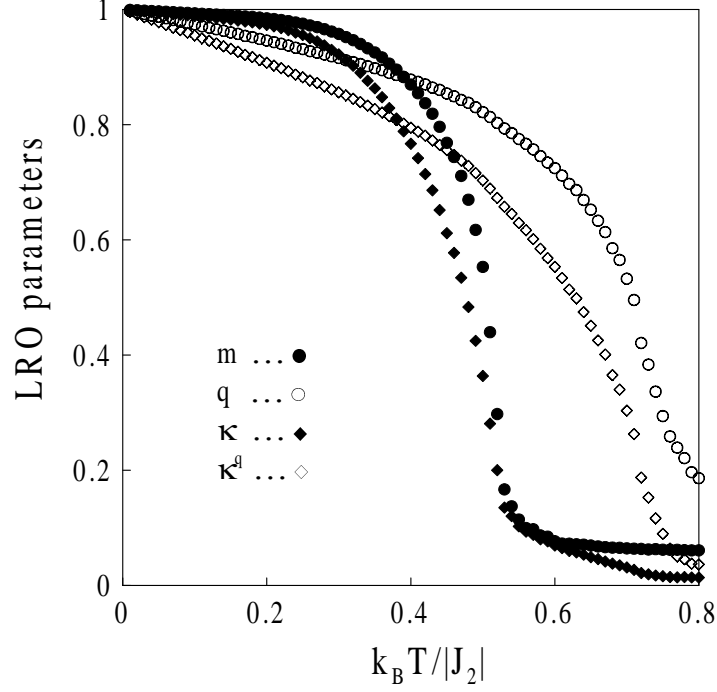


FIG. 7: Temperature variation of the DLRO, QLRO, CHLRO and QCHLRO parameters m , q , κ and κ^q , respectively, for $|J_1|/|J_2| = 0.15$ and $L = 12$.

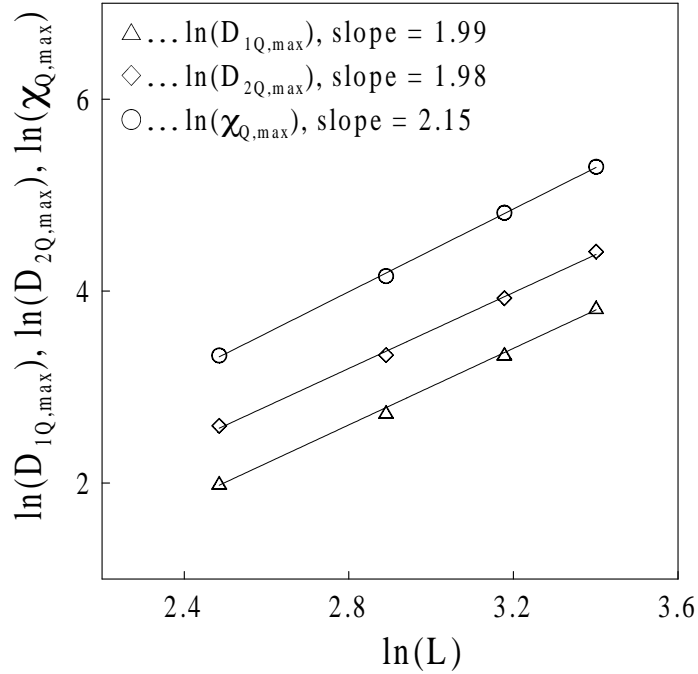


FIG. 8: Scaling behaviour of the maxima of the susceptibility $\chi_{Q,max}$ and logarithmic derivatives of the parameter Q and its second moment $D_{1Q,max}$ and $D_{2Q,max}$, respectively, in \ln - \ln plot, for $|J_1|/|J_2| = 0.15$. The slopes yield values of $1/\nu_Q$ for $D_{1Q,max}$, $D_{2Q,max}$ and γ_Q/ν_Q for $\chi_{Q,max}$.

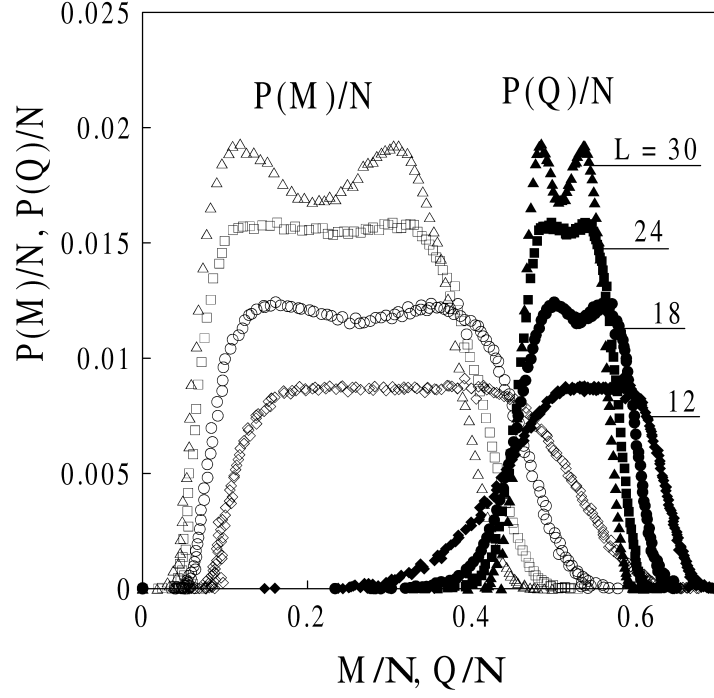


FIG. 9: Distribution histograms $P(M)$ and $P(Q)$ of DLRO and QLRO parameters, respectively, at $T_c(L)$ for $|J_1|/|J_2| = 0.25$. The bimodal distributions of the DLRO and QLRO parameters signal a first-order disorder-DLRO transition and a jump between two finite values of QLRO parameter, respectively (see text).

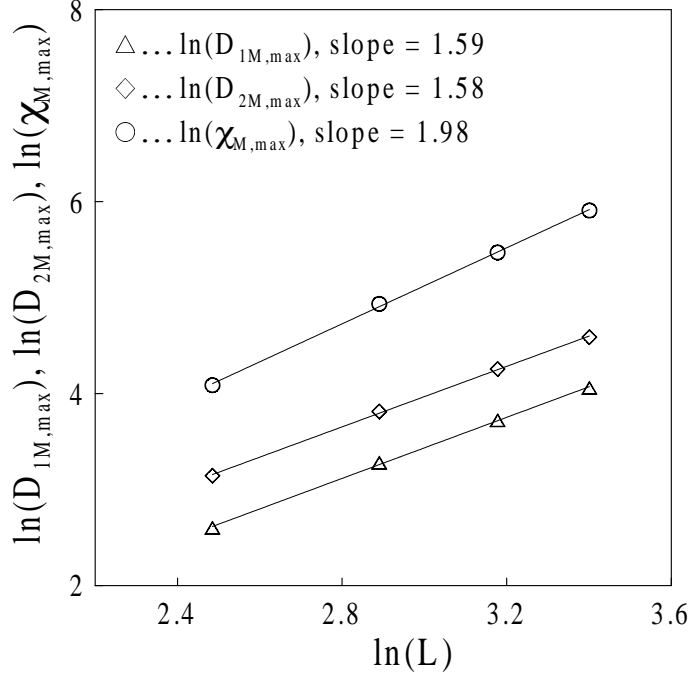


FIG. 10: Scaling behaviour of the maxima of the susceptibility $\chi_{M,max}$ and logarithmic derivatives of the DLRO parameter and its second moment $D_{1M,max}$ and $D_{2M,max}$, respectively, in ln-ln plot, for $|J_1|/|J_2| = 0.15$. The slopes yield values of $1/\nu_M$ for $D_{1M,max}$, $D_{2M,max}$ and γ_M/ν_M for $\chi_{M,max}$.

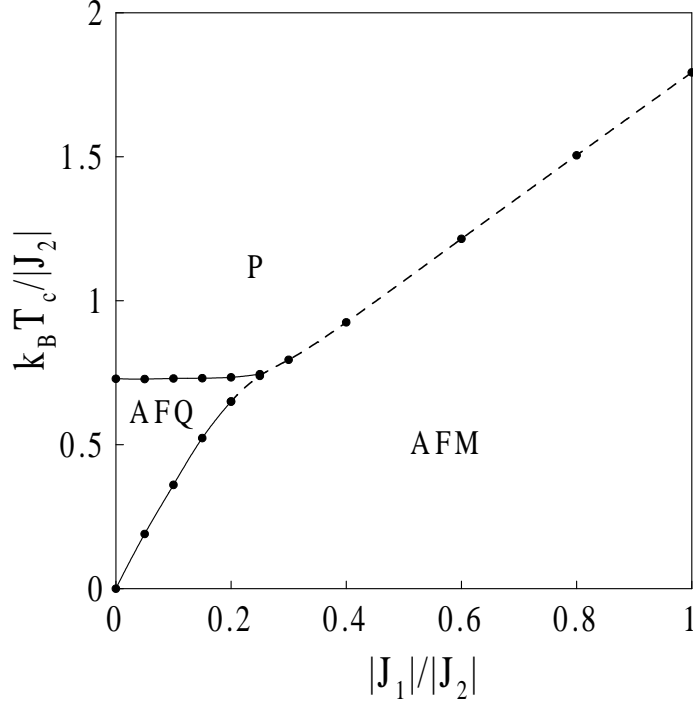
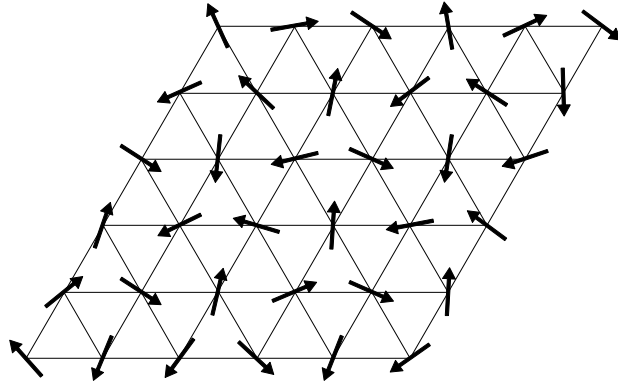
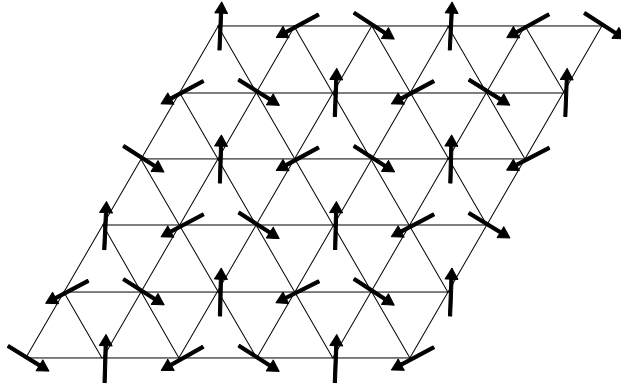


FIG. 11: Phase diagram in $(|J_1|/|J_2|, k_B T_c/|J_2|)$ space. The paramagnetic (P), antiferroquadrupolar (AFQ), and antiferromagnetic (AFM) regions correspond to the phases in which both dipoles and quadrupoles are disordered, only quadrupoles are ordered, and both dipoles and quadrupoles are ordered, respectively. The solid and dashed lines correspond to second- and first-order transitions, respectively.



(a)



(b)

FIG. 12: Spin configuration snapshots of the system for $|J_1|/|J_2| = 0.05$ in (a) QLRO phase ($k_B T/|J_2| = 0.3$) and (b) DLRO phase ($k_B T/|J_2| = 0.001$).